JOURNAL OF GUIDANCE, CONTROL, AND DYNAMICS
Vol. 21, No. 3, May–June 1998

Identification of Autogyro Longitudinal Stability and Control Characteristics

S. S. Houston*
University of Glasgow, Glasgow, Scotland G12 8QQ, United Kingdom

An analysis is presented of test data recorded during flight trials of an autogyro. This class of rotary-wing aircraft has found limited application in areas other than sport or recreational flying. However, the accident rate is such that a study of the configuration's stability and control characteristics is timely, and in addition substantive data is required for a new airworthiness and design standard that is under development. A unique coupling of established parameter estimation techniques with data from a class of aircraft that has received no attention in the contemporary literature is presented. As a consequence, the data help to consolidate the status of system identification as a powerful tool in the analysis of rotorcraft engineering problems. It is concluded that robust estimates of the longitudinal stability and control derivatives have been identified, indicating benign and classical longitudinal stability and control characteristics. However, unlike most helicopters, the rotorspeed degree of freedom must be included in the model structure.

Nomenclature

A, B	= state-space system and control matrices
i	= imaginary operator
M_u, M_w, etc.	= pitching moment derivatives, 1/ms
p, q, r	= angular velocity components about body axes, rad/s
Q_u, Q_w, etc.	= rotor torque derivatives, rev/min/m
R	= regression correlation coefficient
Re[ ], Im[ ]	= real and imaginary components of [ ]
T, T_p	= rotor, propeller thrust, N
$T(u, w)$	= rotor thrust in (u, w) disturbed flight, N
u, w	= velocity components along longitudinal, vertical body axes, m/s
u_{probe}, w_{probe}	= velocity components along longitudinal, vertical air data probe axes, m/s
X_u, X_w, etc.	= longitudinal body axis acceleration derivatives, 1/s
$\boldsymbol{x}$, $\boldsymbol{u}$	= state and control vectors
$\boldsymbol{x}(\omega)$, $\boldsymbol{u}(\omega)$	= Fourier-transformed state and control vectors
x_{cg}, y_{cg}, z_{cg}	= aircraft center-of-mass position in body axes, m
x_{vane}, y_{vane}, z_{vane}	= angle of attack and sideslip vane location in body axes, m
Z_u, Z_w, etc.	= vertical body axis acceleration derivatives, 1/s
α_{vane}, β_{vane}	= angle of attack and sideslip measured at vane location, rad
Δf	= frequency increment, rad/s
Δt	= time increment, s
η_s	= longitudinal stick position (0% fully forward), %
Ω	= rotorspeed, rpm
ω	= frequency, rad/s

Introduction

THERE is a wide range of configurations in the class of aircraft known as rotorcraft. The helicopter is the most common type, finding widespread application in commercial and military aviation. The autogyro (or gyroplane), however, is an increasingly popular machine in sport and recreational flying, having found no practical application in contemporary commercial or military roles.

Currently, most if not all types of autogyro are in the homebuilt, or experimental, category. The study of the configuration's flight mechanics is timely, given the accident rate suffered by the aircraft. For example, Ref. 1 states that between 1989 and 1991, the autogyro fatal accident rate in the United Kingdom was 6 per 1000 flying hours, whereas the overall general aviation rate during 1990 was 0.015 per 1000 flying hours. As a consequence, there is heightened interest in this class of aircraft, and a new airworthiness and design standard (BCAR Section T) has been published by the U.K. Civil Aviation Authority.[2]

However, there are little substantive data at present to support the design standard, and the literature has not, until recently, addressed stability and control.[3] The objective of this paper is, therefore, to contribute to the sparse literature on the subject of autogyro flight mechanics, thereby directly supporting BCAR Section T. The specific aims of the work are to explore the application, to the autogyro, of previous research in rotorcraft system identification; to obtain robust estimates of longitudinal stability and control derivatives; and to use these derivatives to assess the nature of the flight dynamics of autogyros.

Background

The autogyro helped to pave the way for the development of the helicopter, introducing cyclic pitch control and blades attached to the rotor hub by means of a hinge. Unfortunately, with the one exception of Ref. 3, the literature has not hitherto addressed stability and control. The literature on autogyros, nonetheless, is considerable, Refs. 4–14 for example. However, in a contemporary context, this work is now primarily of historical significance. It provides the basis of the understanding of autogyro flight but does not address the issues of stability and control. Examination of the literature shows a logical development of the study of autogyros, from the elementary theory of autogyro flight to an analysis of aerodynamics and performance and ultimately rotor behavior, but only for steady flight. Interest then apparently waned, and the next logical stage in the study of the autogyro, i.e., stability and control, was not examined. For example, the work of Glauert[4] includes the derivation of simple expressions for rotorspeed as a function of loading and axial velocity. Wheatley[10] derived expressions for the flapping angles required for equilibrium flight, presenting results that show how coning and longitudinal and lateral flap angles vary with flight condition. Nowadays, these analyses would be recognizable as classical rotary-wing theory and analogous to that found in helicopter text books. Wheatley[12] even examined higher harmonic components of blade flapping behavior.

It is in this context that autogyro flight trials and the associated data analysis methods were planned. There is an extensive literature on system identification and parameter estimation, and application to the rotorcraft problem is well documented, e.g., Refs. 15–20.

Received Feb. 6, 1997; revision received July 19, 1997; accepted for publication Nov. 18, 1997.

*Lecturer, Department of Aerospace Engineering. Member AIAA.

Tischler,[20] in particular, has argued strongly in favor of the merits of frequency-domain identification, specifically directed toward the synthesis of nonparametric frequency responses. The repeatability and consistency achieved indicate that the frequency-domain approach is robust.

The approach taken in this paper is to adopt a frequency-domain equation-error method using linear regression to synthesize conventional three-degree-of-freedom stability and control derivatives. This model structure is familiar to flight dynamicists, thereby facilitating general insight into fundamental behavior of the autogyro. Specific derivatives are directly related to individual, or group, effects that would otherwise be hidden in the aggregate presentation of a frequency response. The equation-error method has limitations, as described in Refs. 15 and 18, although working in the frequency domain minimizes some of the difficulties. The advantage is the simplicity of the approach in concept and application. It is argued that good results can be obtained with a frequency-domain equation-error approach if careful design of the experiments, the equipment installation, and execution of the flight trials is complemented by sound engineering judgment applied to the interpretation of the data.

Aircraft and Experimental Installation

The aircraft used in this study was the VPM M16 autogyro (Fig. 1). It is of Italian origin, produced in kit form for assembly by the owner. The maximum all-up mass is 450 kg. The aircraft is powered by a four-cylinder two-stroke engine driving a three-bladed fixed pitch propeller. For helicopter engineers not familiar with autogyros, the rotor system is of an interesting configuration, typical of this class of aircraft. The two main rotor blades are bolted to a teeter bar, suspended from a teeter bolt. The blades are untwisted, and no cyclic pitch can be applied. This hub assembly is mounted on a spindle about 200 mm long, and this spindle pivots about its lower end to tilt the entire rotor fore and aft and laterally to effect pitch and roll control, respectively. In this regard, the aircraft could be classed as a tilt rotor.

The experimental installation consisted of a digital on-board recording system, operating at 10 Hz. Antialiasing filters were incorporated. A nose-mounted air data probe containing sideslip and angle-of-attack vanes was fitted, and an inertial unit measured angular velocities about three axes and linear accelerations along these axes. A separate unit was used to measure roll and pitch angles. Pilot control positions were measured using potentiometers. Rotorspeed was also recorded. The front seat and flight controls were removed to accommodate the system. It was found that the aircraft's own indicated airspeed system suffered from a position error of about 8 mph across the speed range. All results are plotted with respect to the indicated airspeed, although the nose-mounted probe data were used for all analysis.

The identification of autogyro dynamics presents a particular challenge, in addition to those normally met with helicopter system identification. The aircraft is light, which demands stringent limits on atmospheric conditions during the tests. Solo operation of this aircraft was essential due to the mass and space restrictions imposed by the instrumentation system. This placed particular demands on the test pilot's flying skills so that the quality of the test inputs were not compromised.

Fig. 1 VPM M16 autogyro with instrumentation system fitted.

Data Analysis and Model Synthesis

The model structure for which coefficients are to be identified, is of conventional state-space form, i.e.,

$$\dot{\boldsymbol{x}} = A\boldsymbol{x} + B\boldsymbol{u} \tag{1}$$

where

$$A = \begin{bmatrix} X_u & X_w & X_q & X_\theta & X_\Omega \\ Z_u & Z_w & Z_q & Z_\theta & Z_\Omega \\ M_u & M_w & M_q & M_\theta & M_\Omega \\ 0 & 0 & 1 & 0 & 0 \\ Q_u & Q_w & Q_q & Q_\theta & Q_\Omega \end{bmatrix}, \qquad B = \begin{bmatrix} X_{\eta_s} \\ Z_{\eta_s} \\ M_{\eta_s} \\ 0 \\ Q_{\eta_s} \end{bmatrix} \tag{2}$$

and

$$\boldsymbol{x} = [u \quad w \quad q \quad \theta \quad \Omega]^T, \qquad \boldsymbol{u} = [\eta_s] \tag{3}$$

This constitutes the longitudinal subset of the conventional six-degree-of-freedom rigid-body flight mechanics model, with the important (and unique) addition of the rotorspeed degree of freedom. The rigid-body states are taken to be with respect to a mutually orthogonal, right-handed frame of reference whose origin is at the center of mass. The longitudinal and vertical axes are parallel and normal to the keel of the aircraft, respectively.

The angular quantities in the state vector and the control position are all measured directly. The translational velocities u and w are obtained from airspeed, sideslip, and angle-of-attack data measured at the nose-mounted boom, as follows:

$$\begin{aligned} u &= u_{\text{probe}} - q(z_{\text{vane}} - z_{\text{cg}}) + r(y_{\text{vane}} - y_{\text{cg}}) \\ w &= w_{\text{probe}} - p(y_{\text{vane}} - y_{\text{cg}}) + q(x_{\text{vane}} - x_{\text{cg}}) \end{aligned} \tag{4}$$

and

$$u_{\text{probe}} = \frac{V_f \cos\beta_{\text{vane}}}{\sqrt{1 + \tan^2\alpha_{\text{vane}}}}, \qquad w_{\text{probe}} = u_{\text{probe}} \tan\alpha_{\text{probe}} \tag{5}$$

The time histories of each variable were then converted into frequency-domain information[20] using a discrete Fourier transform given by

$$X(k\Delta f) = \Delta t \sum_{n=0}^{N-1} x_n \exp\left[\frac{-i2\pi(kn)}{N}\right] \qquad k = 0, 1, 2, \ldots, N-1 \tag{6}$$

which gives real and imaginary parts of X,

$$\begin{aligned} \text{Re}[X(k\Delta f)] &= \Delta t \sum_{n=0}^{N-1} x_n \cos\left(\frac{2\pi(kn)}{N}\right) \\ \text{Im}[X(k\Delta f)] &= -\Delta t \sum_{n=0}^{N-1} x_n \sin\left(\frac{2\pi(kn)}{N}\right) \end{aligned} \tag{7}$$

The quality of these frequency-domain data can be enhanced by standard processing techniques such as applying overlapped and tapered windows to the data, as recommended by Tischler.[20]

Each degree of freedom can then be treated separately, and the formulation as a linear regression problem allows estimation of the coefficients. The state-space description is converted to the frequency domain, i.e.,

$$i\omega\boldsymbol{x}(\omega) = A\boldsymbol{x}(\omega) + B\boldsymbol{u}(\omega) \tag{8}$$

Table 1 Force derivative comparison, dissimilar input types

	X force			Z force	
Parameter	Concatenated doublet/phugoid	Frequency sweep	Parameter	Concatenated doublet/phugoid	Frequency sweep
R	0.742	0.822	R	0.928	0.706
X_u	0.081 (0.056)	0.047 (0.025)	Z_u	−0.060 (0.025)	−0.128 (0.024)
X_w	−0.126 (0.109)	−0.268 (0.058)	Z_w	−0.788 (0.048)	−0.565 (0.057)
X_q	−3.976 (3.499)	−1.169 (1.380)	Z_q	23.665 (1.529)	26.446 (1.350)
X_θ	−9.036 (1.578)	−10.632 (0.851)	Z_θ	2.247 (0.690)	4.060 (0.832)
X_Ω	−0.044 (0.013)	−0.025 (0.006)	Z_Ω	−0.054 (0.005)	−0.065 (0.006)
X_{η_s}	0.010 (0.034)	−0.001 (0.013)	Z_{η_s}	−0.100 (0.015)	−0.098 (0.013)

Table 2 Moment derivative comparison, dissimilar input types

	Pitch moment			Rotor torque	
Parameter	Concatenated doublet/phugoid	Frequency sweep	Parameter	Concatenated doublet/phugoid	Frequency sweep
R	0.919	0.886	R	0.910	0.966
M_u	0.023 (0.003)	0.021 (0.001)	Q_u	1.373 (0.166)	1.378 (0.042)
M_w	−0.065 (0.007)	−0.064 (0.003)	Q_w	5.324 (0.628)	5.901 (0.126)
M_q	−1.213 (0.126)	−1.055 (0.076)	Q_q	12.590 (12.419)	7.679 (3.076)
M_θ	−0.449 (0.181)	−0.294 (0.047)	Q_θ	0–fixed	0–fixed
M_Ω	−0.001 (0.0006)	−0.001 (0.0003)	Q_Ω	−0.129 (0.029)	−0.085 (0.007)
M_{η_s}	0.029 (0.001)	0.028 (0.0007)	Q_{η_s}	0.305 (0.129)	0.314 (0.030)

Note that this assumes that any process noise is zero. The unknown coefficients of the A and B matrices are determined by solutions of the frequency-domain equations

$$-\omega\,\mathrm{Im}[\boldsymbol{x}(\omega)] = A\{\mathrm{Re}[\boldsymbol{x}(\omega)]\} + B\{\mathrm{Re}[\boldsymbol{u}(\omega)]\}$$
$$\omega\,\mathrm{Re}[\boldsymbol{x}(\omega)] = A\{\mathrm{Im}[\boldsymbol{x}(\omega)]\} + B\{\mathrm{Im}[\boldsymbol{u}(\omega)]\} \tag{9}$$

This solution applies equal weighting to real and imaginary part errors, which is consistent with the standard weighting for system identification on a Bode plot. The pitching moment equation, for example, is then expressed as the two equations

$$\begin{aligned}-\omega\,\mathrm{Im}[q(\omega)] &= M_u\mathrm{Re}[u(\omega)] + M_w\mathrm{Re}[w(\omega)] + M_q\mathrm{Re}[q(\omega)] \\ &\quad + M_\theta\mathrm{Re}[\theta(\omega)] + M_\Omega\mathrm{Re}[\Omega(\omega)] + M_{\eta_s}\mathrm{Re}[\eta_s(\omega)] \\ \omega\,\mathrm{Re}[q(\omega)] &= M_u\mathrm{Im}[u(\omega)] + M_w\mathrm{Im}[w(\omega)] + M_q\mathrm{Im}[q(\omega)] \\ &\quad + M_\theta\mathrm{Im}[\theta(\omega)] + M_\Omega\mathrm{Im}[\Omega(\omega)] + M_{\eta_s}\mathrm{Im}[\eta_s(\omega)]\end{aligned} \tag{10}$$

The other degrees of freedom are in a similar form.

Results

The test points were nominal airspeeds of 30, 50, and 70 mph. At each of these speeds, a doublet-type input was used to excite the short-term response, and the standard technique of displacing the stick to provoke a speed change before returning it to trim was used to excite any phugoid. Frequency sweep inputs were conducted only at the 70-mph test point. Figure 2 illustrates a typical frequency sweep. This type of test proved difficult to perform at 30 and 50 mph due to the ineffectiveness of the trim system on the aircraft at airspeeds less than 70 mph. The consequent out-of-trim stick force proved distracting and difficult to compensate for during the conduct of a sweep.

An important aspect in any system identification study is the identifiability of the estimated parameters.[21,22] This is particularly germane to the equation-error approach. Robust estimates of the derivatives are those whose values can be judged to be invariant with the event, input type, estimation method, or frequency range used and for which a low standard error is calculated. Verification of the appropriateness of the identified model is usually achieved by confirming that it will predict the response to a control input dissimilar to that used in the identification. The issue of identifiability is particularly germane to the autogyro problem as there is no literature on the vehicle's characteristics. These issues are explored next.

Derivative Estimates from Dissimilar Input Types

Data from doublet and phugoid tests were zero meaned and concatenated to provide a 90-s record length. The longitudinal derivatives estimated using these data are compared in Tables 1 and 2, with derivatives estimated from a frequency sweep. The standard error associated with each derivative is given in parentheses.

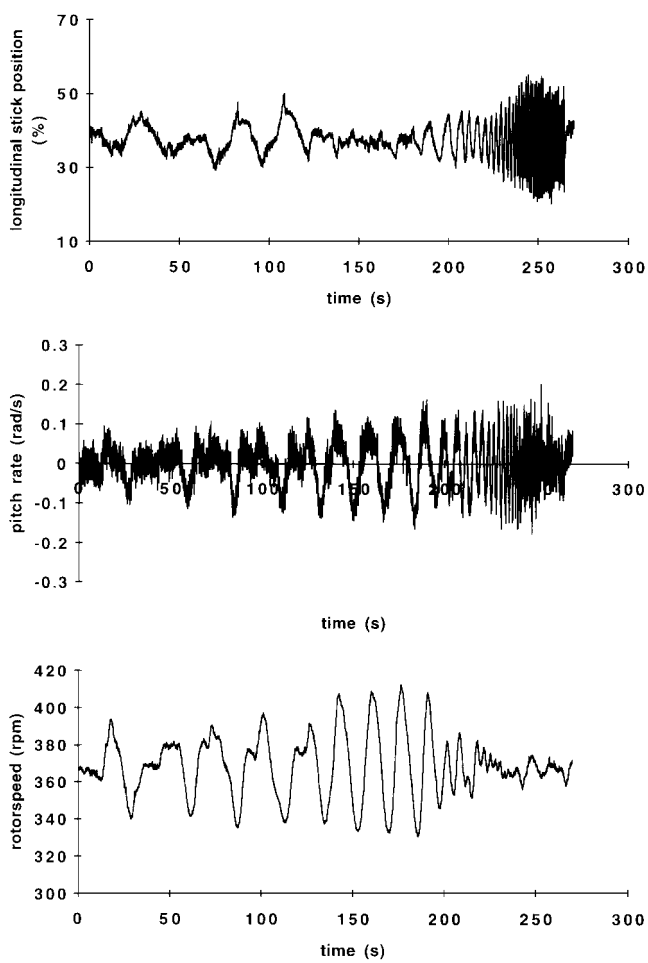

Fig. 2 Response during frequency sweep test at 70 mph.

Consistent estimates of the derivatives are obtained, particularly in the pitching moment and rotor torque equations. The correlation coefficients are also, in general, good. The standard error associated with each estimate is relatively small, although for frequency sweep-derived parameters the errors are generally smaller than with

Table 3 Force derivative comparison, dissimilar regression frequency range

	X force			*Z* force	
Parameter	0.5 Hz	1.0 Hz	Parameter	0.5 Hz	1.0 Hz
R	0.902	0.822	R	0.786	0.706
X_u	0.112 (0.034)	0.047 (0.025)	Z_u	−0.092 (0.029)	−0.128 (0.024)
X_w	−0.248 (0.065)	−0.268 (0.058)	Z_w	−0.621 (0.055)	−0.565 (0.057)
X_q	−6.137 (2.374)	−1.169 (1.380)	Z_q	23.301 (2.003)	26.446 (1.350)
X_θ	−10.467 (0.852)	−10.632 (0.851)	Z_θ	3.489 (0.719)	4.060 (0.832)
X_Ω	−0.025 (0.006)	−0.025 (0.006)	Z_Ω	−0.061 (0.005)	−0.065 (0.006)
X_{η_s}	0.053 (0.024)	−0.001 (0.013)	Z_{η_s}	−0.047 (0.021)	−0.098 (0.013)

Table 4 Moment derivative comparison, dissimilar regression frequency range

	Pitch moment			Rotor torque	
Parameter	0.5 Hz	1.0 Hz	Parameter	0.5 Hz	1.0 Hz
R	0.897	0.886	R	0.984	0.966
M_u	0.021 (0.001)	0.021 (0.001)	Q_u	1.535 (0.063)	1.378 (0.042)
M_w	−0.043 (0.003)	−0.064 (0.003)	Q_w	6.319 (0.133)	5.901 (0.126)
M_q	−1.199 (0.093)	−1.055 (0.076)	Q_q	−9.061 (5.036)	7.679 (3.076)
M_θ	−0.203 (0.033)	−0.294 (0.047)	Q_θ	0–fixed	0–fixed
M_Ω	−0.001 (0.0002)	−0.001 (0.0003)	Q_Ω	−0.073 (0.007)	−0.085 (0.007)
M_{η_s}	0.023 (0.001)	0.028 (0.0007)	Q_{η_s}	0.390 (0.052)	0.314 (0.030)

the concatenated doublet/phugoid. Although the force derivative estimates display less consistency than the pitching moment and rotor torque estimates, this is consistent with parameter estimation experience in general, where force derivatives have been more difficult to identify than moment derivatives. However, it is argued that these force derivative estimates are consistent to within the statistical error bounds associated with each derivative. The standard errors indicate that the corresponding derivatives will lie within the 95% confidence bounds associated with their respective estimates.

Derivatives that physically ought to have negligible aerodynamic or propulsion force and moment contributions, i.e., those dominated by kinematic or gravitational terms, are X_θ and Z_q. The former ought to have a value of approximately −9.81. Both input types give estimates of X_θ and Z_q that are very similar, and in the case of Z_q also are consistent with the mean flight speed of 28 m/s. This enhances confidence in the frequency sweep-derived Z-force derivatives, despite this equation providing the lowest correlation coefficient. Note that terms normally expected to be negligible or zero, such as Z_θ and M_θ, were retained in the regression as an additional check on model structure validity. Z_θ is not negligible, although it is estimated with a relatively large standard error, and removing it from the regression proved to have little impact on the goodness of fit or the other parameters in the model. Removing M_θ from the pitching moment model also had little effect on the other estimates, although it is estimated with a relatively low standard error, tending to suggest that it should be retained. However, its contribution to the overall pitch moment is approximately an order of magnitude smaller than the other terms in the equation, for the perturbations in $\boldsymbol{x}$ and $\boldsymbol{u}$ experienced in flight.

Estimates for the X-force derivative X_u are very small, with relatively large standard error. Note that both estimates are positive. This parameter is the primary damping term in the phugoid mode,[23] and it would normally be expected to be substantially negative. As will be seen later, inspection of the airspeed time histories suggests consistency with the identified values of X_u, in that there is little apparent damping of airspeed during the longer term, phugoid-type oscillation.

The pitching moment derivatives M_u, M_w, and M_q describe an aircraft with classical longitudinal stability characteristics. Speed stability is positive ($M_u > 0$), angle-of-attack stability is positive ($M_w < 0$), and the primary pitch damping is positive ($M_q < 0$). Figure 3 shows a comparison of the identified pitching moment equation's fit of the Fourier-transformed frequency sweep data. The fit is good across the frequency range used for the regression.

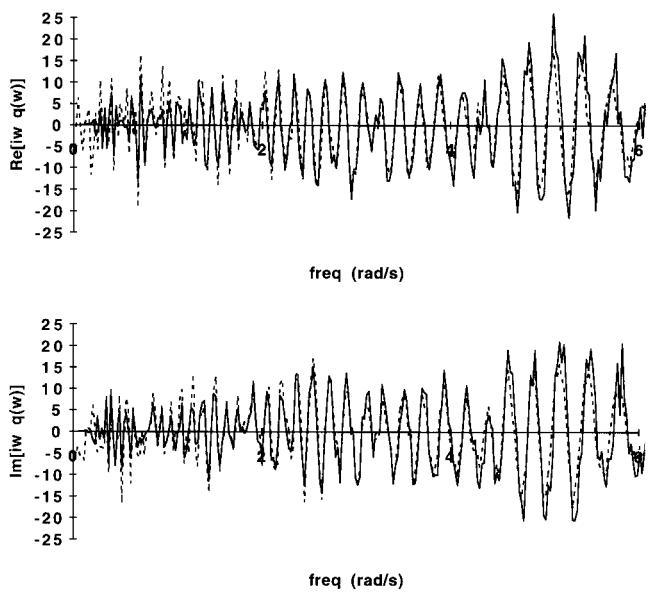

Fig. 3 Fit quality of flight and identified model pitching moment equation: —— and - · · -, flight, and – – –, identified model.

Derivative Estimates from Fits over Dissimilar Frequency Ranges

Suitable choice of frequency range across which the identification is to be conducted is important for two reasons. First, with too small a frequency range, insufficient information may be available to fully specify the parameters in the model structure. Second, with too large a frequency range, dynamics unmodeled by the four-degree-of-freedom structure may distort the values. Derivative estimates from the frequency sweep data were obtained for regressions over the frequency ranges of 0–0.5 Hz and 0–1 Hz, and these results are compared in Tables 3 and 4.

The pitching moment and rotor torque derivatives show little variability with the frequency range used. The force derivatives show some variation, but it is not significant enough to produce substantially dissimilar dynamic characteristics. Concern that unmodeled rotor dynamics may be distorting the derivative estimates obtained for the 1-Hz regression is allayed by the pitching moment derivatives, which are arguably the most sensitive to these effects. Parameter estimates and standard errors are very similar in both cases.

Verification

Figure 4a shows verification of a model identified from frequency sweep data. The model is driven by a doublet-type input made at the same nominal flight condition of 70 mph. The doublet-type input was used specifically to excite the short-term response, where the dominant variables were observed to be pitch rate and rotorspeed.

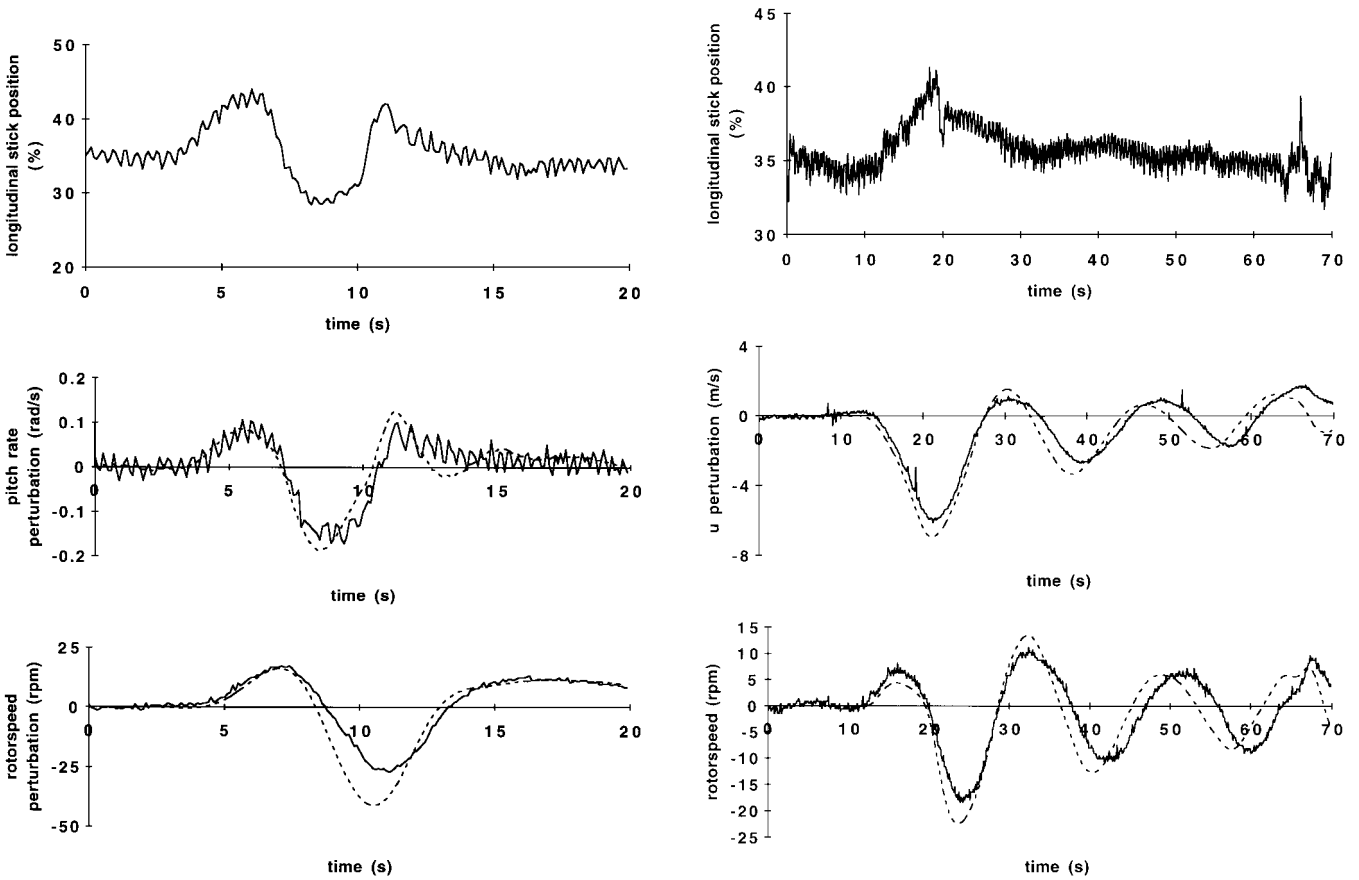

a) Short-term response **b) Long-term response**

Fig. 4 Identified model verification, 70 mph: ——, measurement, and – – –, identified model.

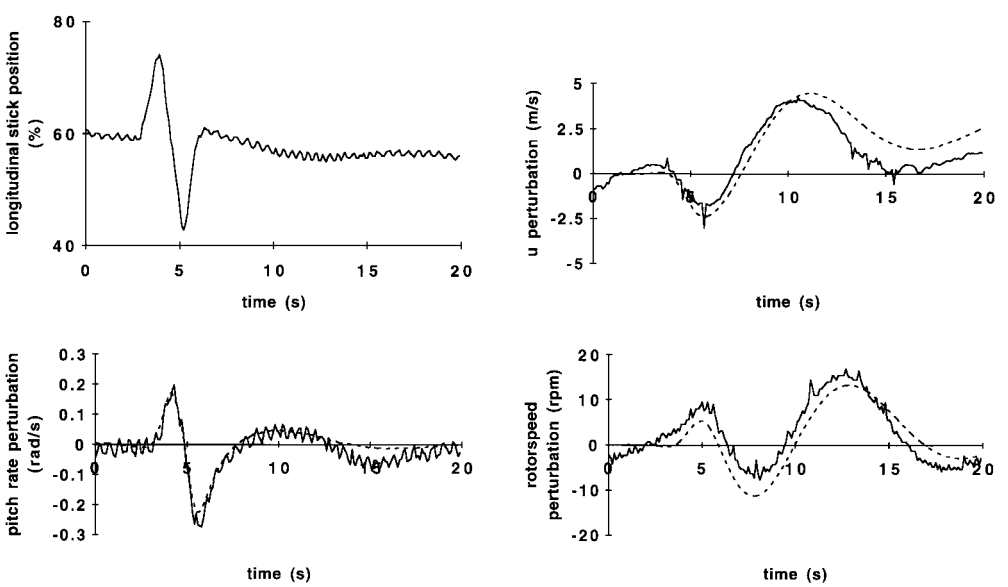

Fig. 5 Identified model verification, 30 mph: ——, measurement, and – – –, identified model.

The identified model provides a very good representation of the response, but displays a feature common to verification with other runs in that any mismatch between identified model and measurement is associated with reduction in rotorspeed.

Figure 4b shows the model's ability to simulate measured behavior during a phugoid test. Amplitude and phase of the u velocity and rotorspeed components of the phugoid mode are well represented by the identified model. The slight mismatch in the long-period response is a consequence of the model result being shifted in time by about 2 s relative to the measured response. This is perhaps not surprising, for two reasons. First, the correlation coefficients shown earlier indicate that the model structure may only approximate observed behavior. Second, the input required for this test produced a very substantial reduction in airspeed, which may take the identified model out of its limit of applicability. Notwithstanding this, the model does capture the substantial reduction in airspeed and rotorspeed before the control is returned to trim.

Unlike the 70-mph test point, the doublet-type input is sufficient to excite longer term as well as short-term responses at 30 mph. This is shown in Fig. 5, which compares the response predicted by

the identified model for 30 mph. This model captures the salient features of the response, giving added confidence that concatenated doublet/phugoid test inputs can be used for identification.

Assessment of Autogyro Longitudinal Flight Dynamics

The foregoing provides a qualitative and quantitative basis for the judgment that the identified models provide a good representation of the longitudinal flight dynamics of the VPM M16 autogyro. It is argued that they can, therefore, be used to assess the nature of the type's stability and controllability characteristics.

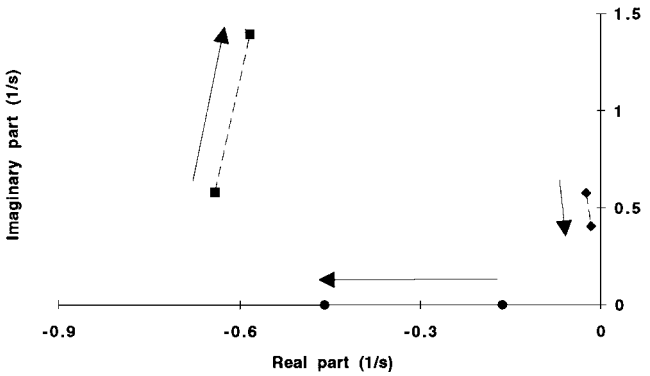

Fig. 6 Identified model eigenvalues, 30 and 70 mph: ■, short-period; ●, rotorspeed; and ♦, phugoid.

Figure 6 shows the eigenvalues of the synthesized models at 30 and 70 mph. The arrows indicate the progression from low to high speed. The two oscillatory modes are consistent with the frequency and damping of classical fixed-wing aircraft short-period and phugoid oscillations. The aperiodic mode is that of the rotorspeed degree of freedom. Assessment of the eigenvectors of the identified A matrices indicates that rotorspeed also features significantly in the rigid-body modes. The phugoid mode is relatively insensitive to changes in airspeed. The time to half-amplitude is about 30–40 s; its period is 12–15 s. The short-period mode is less than critically damped throughout the speed range, with a damped natural frequency of between 0.1 and 0.25 Hz. The rotorspeed mode time to half-amplitude lies between 1 and 4 s.

Figure 7 presents the 95% confidence/95% probability bounds of those identified derivatives that tend to determine fundamentally the dynamic characteristics. The relatively wide boundaries associated with X_u and the small or even positive identified values are possibly due to the lack of propeller speed variations in the model structure. The other derivative estimates all exhibit much narrower bounds. The aircraft exhibits classical static stability characteristics ($M_u > 0$, $M_w < 0$, and $M_q < 0$) across the speed range and not just at 70 mph as noted earlier. The derivative unique to the autogyro is M_Ω and, being negative, will tend to be stabilizing. This is because an increase in rotorspeed will result in a nose-down moment, tending to reduce the axial flow through the rotor and, hence, tending to reduce the original rotorspeed disturbance.

M_u is an indication of the speed stability of the aircraft, and the exhibited trend is consistent with the measured longitudinal stick

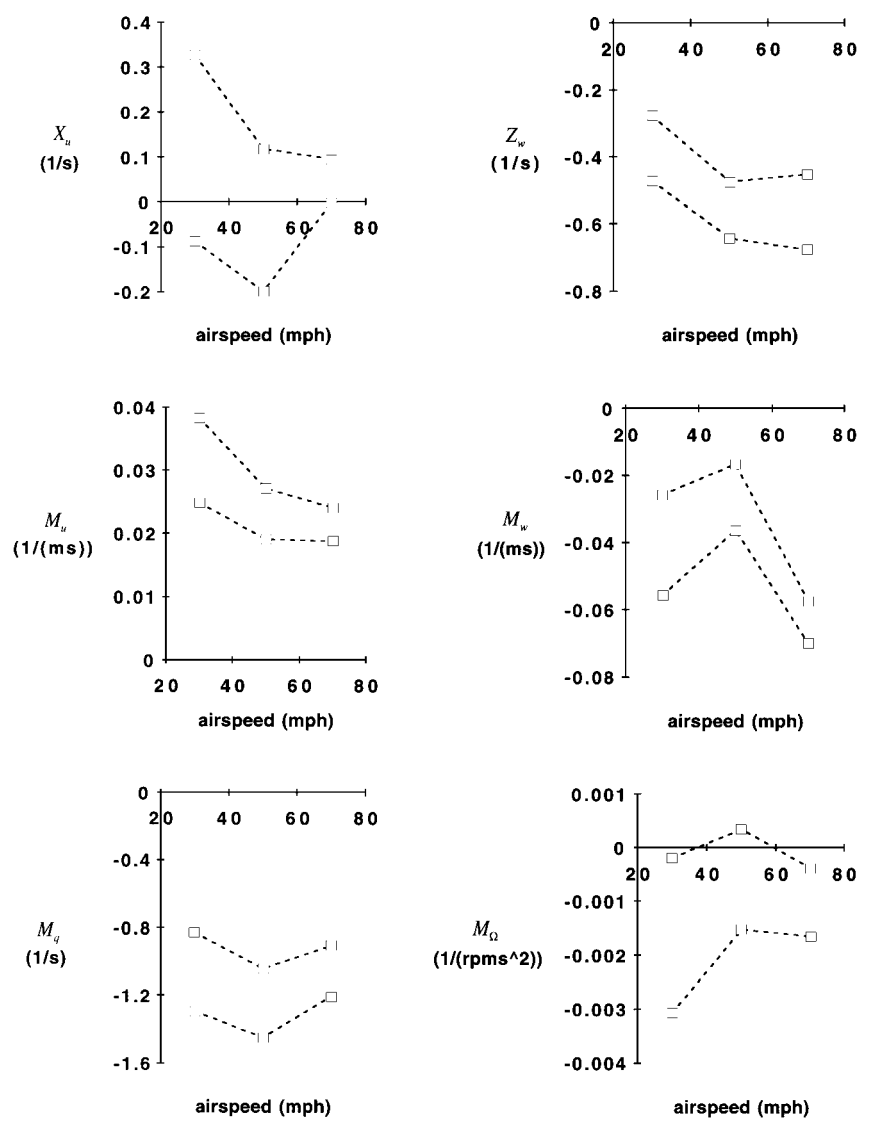

Fig. 7 Key identified force and pitching moment derivatives.

position in trimmed flight. Unmodeled propeller speed and, hence, thrust variations may very well have a role to play in this derivative, quite apart from the usual rotor and tailplane contributions. M_w is the angle-of-attack stability, and unusually for a rotorcraft, it is negative throughout the speed range. This is an important derivative as it holds the clue to a general understanding of autogyro flight dynamics. Unaugmented rotorcraft generally rely on a horizontal tailplane to provide $M_w < 0$. This is because the natural tendency of the rotor (and hence thrust vector) is to flap back with angle-of-attack or w disturbances. Because rotor thrust also increases with w and the thrust line usually passes close to the center of mass in undisturbed flight, both effects sum to produce $M_w > 0$ (Ref. 24). However, the profile of M_u and M_q with speed would tend to suggest that the tailplane on this autogyro is somewhat ineffective, despite its relatively large size. This is consistent with wind-tunnel tests on this configuration.[25] Pusher propeller configurations will tend to produce a stabilizing contribution to M_w as a consequence of the propeller normal force increasing with angle-of-attack disturbances. However, the relatively low power of the engine would suggest that this effect is small, and if considered with the very unclean aerodynamic environment in which the propeller operates, renders this phenomenon difficult to quantify.

Reference 3 postulated that autogyro longitudinal stability could be dominated by the vertical position of the center of mass relative to the propeller thrust line, and a configuration with propeller thrust line below the center of mass could exhibit $M_w < 0$ even at low airspeeds where any tailplane contribution would be negligible. The mechanism for this is shown in Fig. 8. The nose-up moment produced by a configuration with propeller thrust line below the center of mass will need to be trimmed in equilibrium flight by having the main rotor thrust line passing behind the center of mass as shown. In disturbed flight then the possibility exists of the reduction in nose-down moment, caused by the rotor flapping back, being overcome by the contribution from the increase in thrust, resulting in $M_w < 0$. Note that the result $M_\Omega < 0$ identified here is also consistent with such a configuration. Calculations based on mass and balance measurements do place the vertical position of the center of mass 0.02 m above a line passing through the center of the propeller hub. Further validation of this postulate comes from the marked reduction in M_w (and M_Ω) at 50 mph. This is close to the minimum drag speed and, hence, is where the propeller thrust would be a minimum also. Any pitching moment from the propeller would, therefore, be a minimum, and the main rotor thrust line would be at its closest to the center of mass in equilibrium flight, i.e., tending to give a smaller M_w than at the higher power speeds of 30 and 70 mph.

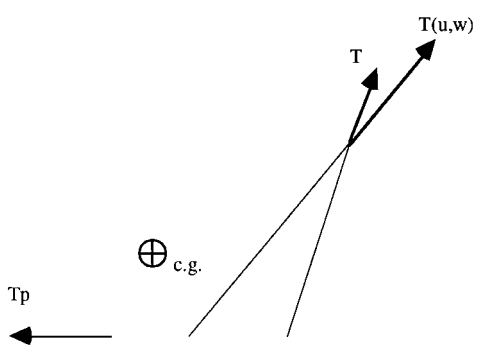

Fig. 8 Rotor and propeller forces in equilibrium and disturbed flight.

Figure 9 shows three estimates for M_w at each speed, obtained from different flights. The multirun consistency exhibited serves to confirm $M_w < 0$ throughout the speed range, even at low speed, and also to confirm the observed effect that M_w is reduced in magnitude at around the minimum drag speed.

Figure 10 shows the identified derivatives in the rotor torque equation. It is impossible to relate these to any previous quantitative work. However, qualitatively Q_u and Q_w are consistent with Glauert's seminal work[4] in that an increase in airspeed and axial velocity will both tend to increase rotorspeed ($Q_u > 0$, $Q_w > 0$). Although the primary damping term Q_Ω decreases with airspeed, the rotorspeed mode itself exhibits the opposite trend (Fig. 6). This indicates the extent of intermodal coupling between the rotorspeed and body degrees of freedom. Finally, the control derivative Q_{η_s} shows that the rotorspeed response will become increasingly sensitive to control application with airspeed.

Discussion

These results are significant for several reasons. First, they are unique in that the literature indicates that no previous in-flight investigation of autogyro stability and control has taken place. Second, the results are timely in that the United Kingdom autogyro accident record is poor, and a substantial number of fatal accidents remain largely unexplained. In addition, the United Kingdom's new airworthiness and design standard BCAR Section T is a unique code and requires substantive data, having been developed largely from other codes. Third, contemporary flight test and data analysis techniques have been used, which helps to consolidate the status of system identification and parameter estimation for rotorcraft. The autogyro joins conventional single main and tail rotor helicopters, tandem rotor helicopters, and tilt rotors as rotorcraft that have enjoyed the successful application of these tools to a real engineering problem.

Although the results obtained are specific to the VPM M16 autogyro, they are of more general significance for two reasons. First, as autogyro stability and control have not been featured in the literature

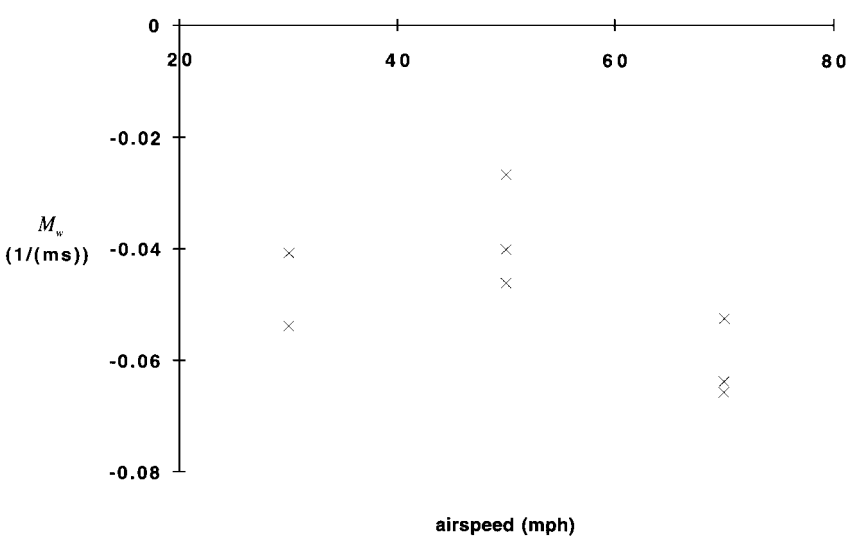

Fig. 9 Multirun consistency of results in M_w.

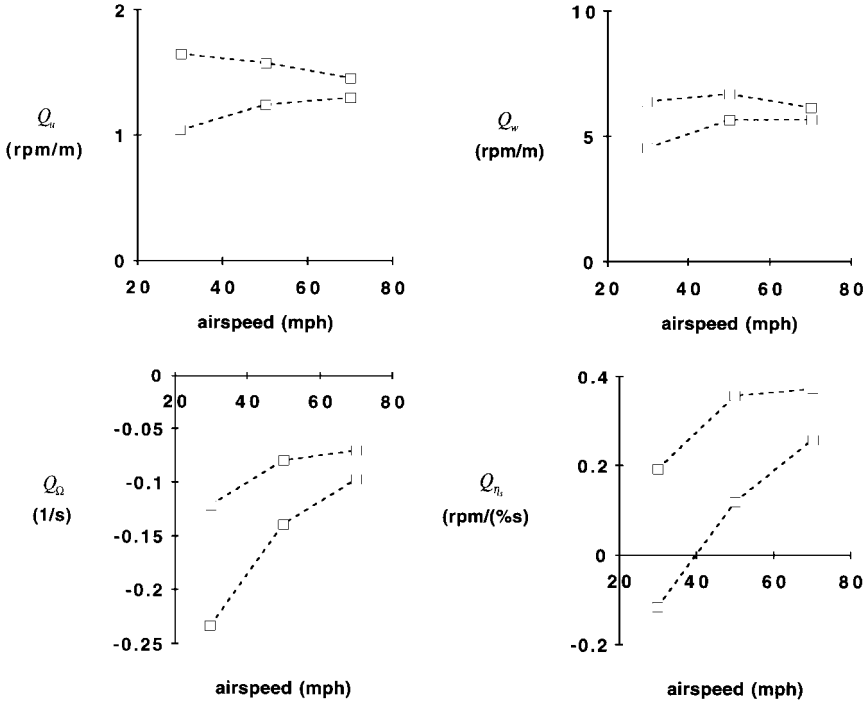

Fig. 10 Rotor torque derivatives.

until recently, cataloging the characteristics of one type of autogyro benchmarks the quantification of autogyro stability in general. Second, the result in M_w in particular can be rationalized in terms of center-of-mass position with respect to propeller thrust line, an issue of direct relevance to all autogyros. The results can also be applied directly to the development of the airworthiness and design standard BCAR Section T, as they constitute the only documentation of actual aircraft characteristics to date. For example, there is no requirement for balance to be specified in terms of vertical center-of-mass position in relation to the propeller thrust line. The results suggest that this is an important consideration in conferring positive angle-of-attack stability M_w, which it is relatively easy to show has a key role to play in stabilizing the phugoid mode of rotorcraft.[23]

Finally, the results quantify the extent to which the rotorspeed degree of freedom is significant in autogyro flight mechanics. The pilot relies on management of flight state to maintain rotorspeed, having no direct control over it. Although the results indicate that the rotorspeed mode is stable, it is closely coupled with the conventional rigid-body degrees of freedom. The rotor torque derivatives indicate that rotorspeed is sensitive to airspeed and angle-of-attack perturbations, and this may have implications for handling in marginal situations.

Conclusions

Robust identification of autogyro longitudinal stability and control derivatives has been possible using relatively straightforward frequency-domain parameter estimation tools.

Unusual for rotorcraft in general, the type examined displays classical longitudinal dynamic stability characteristics and is stable throughout the speed range. However, rotorspeed is an important variable and is closely coupled with the conventional rigid-body degrees of freedom.

Interpretation of the identified stability derivatives indicates that the vertical position of the center of mass in relation to the propeller thrust line may have an important role to play in autogyro longitudinal stability.

The results contribute directly to the development of the United Kingdom's autogyro airworthiness and design standard, BCAR Section T, in the important areas of dynamic stability and weight and balance.

Acknowledgments

This work was conducted for the U.K. Civil Aviation Authority under Research Contract 7D/S/1125. The Technical Authority was David Howson.

References

[1]"Airworthiness Review of Air Command Gyroplanes," Air Accidents Investigation Branch Rept., Farnborough, England, UK, Sept. 1991.

[2]"British Civil Airworthiness Requirements, Section T, Light Gyroplane Design Requirements," U.K. Civil Aviation Authority, Paper T 860, Issue 2, Gatwick, England, UK, July 1993.

[3]Houston, S. S., "Longitudinal Stability of Gyroplanes," *Aeronautical Journal*, Vol. 100, No. 991, 1996, pp. 1–6.

[4]Glauert, H., "A General Theory of the Autogyro," Aeronautical Research Committee Repts. and Memoranda 1111, Nov. 1926.

[5]Lock, C. N. H., "Further Development of Autogyro Theory Parts I and II," Aeronautical Research Committee Repts. and Memoranda 1127, March 1927.

[6]Glauert, H., "Lift and Torque of an Autogyro on the Ground," Aeronautical Research Committee Repts. and Memoranda 1131, July 1927.

[7]Lock, C. N. H., and Townend, H. C. H., "Wind Tunnel Experiments on a Model Autogyro at Small Angles of Incidence," Aeronautical Research Committee Repts. and Memoranda 1154, March 1928.

[8]Glauert, H., and Lock, C. N. H., "A Summary of the Experimental and Theoretical Investigations of the Characteristics of an Autogyro," Aeronautical Research Committee Repts. and Memoranda 1162, April 1928.

[9]Wheatley, J. B., "Wing Pressure Distribution and Rotor-Blade Motion of an Autogyro as Determined in Flight," NACA TR 475, Jan. 1933.

[10]Wheatley, J. B., "An Aerodynamic Analysis of the Autogyro Rotor with a Comparison Between Calculated and Experimental Results," NACA TR 487, Jan. 1934.

[11]Wheatley, J. B., and Hood, M. J., "Full-Scale Wind-Tunnel Tests of a PCA-2 Autogyro Rotor," NACA TR 515, Jan. 1935.

[12]Wheatley, J. B., "An Analytical and Experimental Study of the Effect of Periodic Blade Twist on the Thrust, Torque and Flapping Motion of an Autogyro Rotor," NACA TR 591, Jan. 1937.

[13]Schad, J. L., "Small Autogyro Performance," *Journal of the American Helicopter Society*, Vol. 10, No. 3, 1965, pp. 39–43.

[14]McKillip, R. M., and Chih, M. H., "Instrumented Blade Experiments Using a Light Autogyro," *Proceedings of the 16th European Rotorcraft Forum* (Glasgow, Scotland, UK), 1990.

[15]Fu, K.-H., and Marchand, M., "Helicopter System Identification in the Frequency Domain," *Proceedings of the 9th European Rotorcraft Forum* (Stresa, Italy), 1983.

[16]Tischler, M. B., Fletcher, J. W., Diekmann, V. L., Williams, R. A., and Cason, R. W., "Demonstration of Frequency-Sweep Testing Technique Using a Bell 214-ST Helicopter," NASA TM-89422, April 1987.

[17]Tischler, M. B., "Frequency-Response Identification of XV-15 Tilt-Rotor Aircraft Dynamics," NASA TM-89428, May 1987.

[18]de Leeuw, J. H., "Identification Techniques, Model Structure and Time Domain Methods," AGARD LS178, Oct. 1991, pp. 5-1–5-9.

[19]Kaletka, J., "Instrumentation and Data Processing," AGARD LS178, Oct. 1991, pp. 3-1–3-18.

[20]Tischler, M. B., "Identification Techniques, Frequency Domain Methods," AGARD LS178, Oct. 1991, pp. 6-1–6-4.

[21]Houston, S. S., and Black, C. G., "On the Identifiability of Helicopter Models Incorporating Higher-Order Dynamics," *Journal of Guidance, Control, and Dynamics*, Vol. 14, No. 4, 1991, pp. 840–847.

[22]Murray-Smith, D. J., "Modelling Aspects and Robustness Issues in Rotorcraft System Identification," AGARD LS178, Oct. 1991, pp. 6-1–6-4.

[23]Padfield, G. D., "On the Use of Approximate Models in Helicopter Flight Mechanics," *Vertica*, Vol. 5, No. 3, 1981, pp. 243–259.

[24]Bramwell, A. R. S., *Helicopter Dynamics*, Arnold, London, 1976, pp. 199, 200.

[25]Coton, F., Smrcek, L., and Pátek, Z., "Aerodynamic Characteristics of a Gyroplane Configuration," *Journal of Aircraft*, Vol. 35, No. 2, 1998, pp. 274–279.